

Article

Source/Load-Pull Noise Measurements at K_a Band

Sergio Colangeli ^{1,*}, Walter Ciccognani ¹, Patrick Ettore Longhi ¹, Lorenzo Pace ¹, Antonio Serino ¹, Julien Poulain ², Rémy Leblanc ² and Ernesto Limiti ¹

¹ Electronics Engineering, University of Roma Tor Vergata, Via del Politecnico 1, 00133 Roma, Italy; ciccognani@ing.uniroma2.it (W.C.); longhi@ing.uniroma2.it (P.E.L.); pace@ing.uniroma2.it (L.P.); serino@uniroma2.it (A.S.); limiti@ing.uniroma2.it (E.L.)

² OMMIC SAS, 2 Rue du Moulin, 94453 Limeil Brévannes, France; j.poulain@ommic.com (J.P.); r.leblanc@ommic.com (R.L.)

* Correspondence: colangeli@ing.uniroma2.it; Tel.: +39-7259-7268

Abstract: This paper is focused on the extraction of the noise parameters of a linear active device by exploiting both forward and reverse noise power measurements associated with different terminations. In order for load-pull measurements to yield a significant marginal improvement (as compared to forward measurements only) it is expected that the device under test should appreciably deviate from unidirectionality. For this reason, the source/load-pull technique is applied to frequencies at which the considered devices are still usable but their reverse noise factor exhibits a measurable dependence on the output terminations. Details on the test bench set up to the purpose, covering the 20–40 GHz frequency range, are provided. A characterization campaign on a 60 nm gate length, 4 × 35 μm GaN-on-Si HEMT fabricated by OMMIC is illustrated.

Keywords: black-box modeling; cold-source technique; Gallium Nitride on Silicon; HEMT; noise characterization; source pull; Y-factor technique



Citation: Colangeli, S.; Ciccognani, W.; Longhi, P. E.; Pace, L.; Serino, A.; Poulain, J.; Leblanc, R.; Limiti, E. Source/Load-Pull Noise Measurements at K_a Band. *Energies* **2021**, *14*, 5615. <https://doi.org/10.3390/en14185615>

Academic Editor: Eugenio Meloni

Received: 29 July 2021

Accepted: 3 September 2021

Published: 7 September 2021

Publisher's Note: MDPI stays neutral with regard to jurisdictional claims in published maps and institutional affiliations.



Copyright: © 2021 by the authors. Licensee MDPI, Basel, Switzerland. This article is an open access article distributed under the terms and conditions of the Creative Commons Attribution (CC BY) license (<https://creativecommons.org/licenses/by/4.0/>).

1. Introduction

The noise behavior of a linear noisy 2-port network can be fully characterized in terms of four noise parameters, as known from well established theory [1,2]. If the 2-port network is an active device and its small-signal equivalent circuit model is available, those parameters can be determined indirectly: namely, the noise temperatures of the equivalent circuit element are actually extracted [3,4], then the noise parameters are computed [5]. In the absence of a suitable model, on the other hand, a black-box characterization becomes necessary, which has long been performed by means of source-pull noise measurements [6,7] and, more recently, has been also carried out by source/load pull [8–10].

It is worth noting that the noise temperature-based methods can benefit from source- or source/load-pull noise measurements, but they strictly require one physical termination only, although used across a broad frequency range. Black-box methods, on the other hand, require a set of different terminations at each frequency, which are usually obtained by means of electro-mechanical RF tuners [11,12]. Tuners allow to synthesize virtually arbitrary terminations, which can be exploited to optimize the pattern of terminations at each extraction frequency [13–15]. Nevertheless, electro-mechanical tuners are rather costly and may present repeatability issues, so that alternatives have also been proposed, such as custom tuners [6], long lines [16,17] and switching over a set of different physical terminations [18,19]. When switching is adopted, the number of terminations is of course limited by the complexity of the available switching matrix and by the associated loss.

In this paper, several of the previous ideas are reappraised and combined. First of all, a black-box approach is considered, with a small number (only four) of different terminations realized through electro-mechanical switching. To relieve this minimal condition, both forward and reverse noise measurements are taken, thus realizing a source/load pull. Finally, the idea of exploiting measurements at multiple frequencies to produce an extraction at a

single nominal frequency is adopted to further increase the number of *effective* (as opposed to *physical*) terminations. This is justified if the noise correlation matrix can be linearized within some frequency interval. Notice, however, that no assumption is made about the behavior of the source terminations, as opposed to [16,17].

The proposed approach is applied to the black-box on-wafer characterization of a field-effect transistor realized in OMMIC's 60 nm gate length GaN-on-Si HEMT technology (D006GH) [20]. The preliminary assessment of that process is one of the objectives of the MiGaNSOS project [21], funded by the European Commission. Other goals are the space-qualification of the analogous 100 nm process and demonstrating that both can be simultaneously used on the same chip [22,23].

The projects also aims at demonstrating future applications of the developed technologies in advanced space equipment. Due to the growing interest in the K_a band for space applications, such as telecommunications and Earth observation [24,25], a K_a-band synthetic aperture radar (SAR) antenna has been taken as a reference in MiGaNSOS for the design of the test vehicles. More specifically, the project aims at the full integration of a single-chip front-end (SCFE) monolithic microwave integrated chip (MMIC) demonstrator replicating the basic building block of an active antenna operating in the 35–36.5 GHz frequency range [22,26,27].

2. Materials and Methods

2.1. Formalism of Forward and Reverse Noise Measurements

Consider a generic linear noisy 2-port terminated in a source admittance $Y_S = G_S + jB_S$ (associated with a noise temperature T_S) and thus presenting an output admittance $Y_{out} = G_{out} + jB_{out}$ (its noise temperature being T_{out}). It is well known that the small-signal and noise behavior at a given frequency f_0 of such a 2-port can be modeled as the cascade of:

- a noisy thru (fully characterized by a noise correlation matrix), and
- a noiseless 2-port (fully characterized by a small-signal matrix),

as depicted on the left side of Figure 1. Here the expression 'noisy thru' denotes an ideal 2-port network made up of a series noise voltage generator and a shunt noise current generator, such as the one enclosed between sections *s-F1* and *s-Fi* in the figure. In general, the two generators are partially correlated, which is quantified by way of a correlation admittance Y_γ :

$$i_n = Y_\gamma e_n + i_u \quad (1)$$

$$\overline{e_n i_u^*} = 0. \quad (2)$$

In this framework, it is convenient to express the small-signal behavior of the noisy 2-port in the transmission (ABCD) representation. The associated form of the noise correlation matrix is as follows:

$$\mathbf{C} = \begin{bmatrix} e_n \\ i_n \end{bmatrix} \cdot \begin{bmatrix} e_n \\ i_n \end{bmatrix}^H = \begin{bmatrix} \overline{e_n e_n^*} & \overline{e_n i_n^*} \\ \overline{i_n e_n^*} & \overline{i_n i_n^*} \end{bmatrix} = \begin{bmatrix} c_{11} & c_{12} \\ c_{21} & c_{22} \end{bmatrix} = \begin{bmatrix} c_{11} & c_{12} \\ c_{12}^* & c_{22} \end{bmatrix}, \quad (3)$$

where the H superscript denotes the Hermitian operator (transpose and conjugate). It proves useful to normalize \mathbf{C} to $4k_B T_0 B$, where $k_B = 1.3806488 \cdot 10^{-23} \text{ m}^2 \text{ kg s}^{-2} \text{ K}^{-1}$ is Boltzmann's constant, $T_0 = 290 \text{ K}$ is the standard noise temperature and B is the equivalent noise bandwidth:

$$\hat{\mathbf{C}} = \frac{1}{4k_B T_0 B} \mathbf{C}, \quad \hat{c}_{ij} = \frac{1}{4k_B T_0 B} c_{ij}. \quad (4)$$

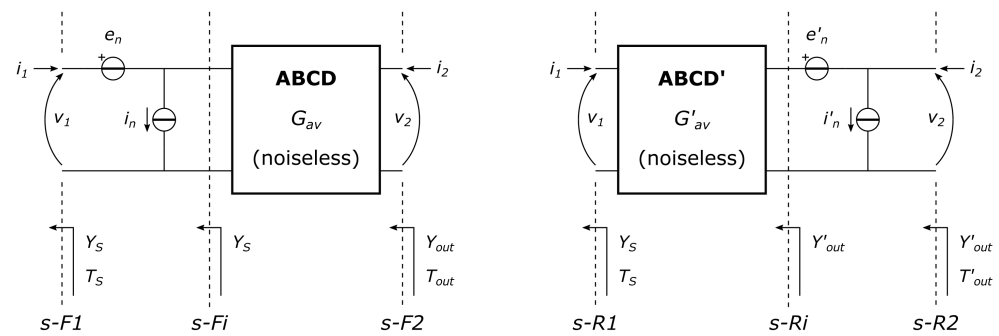


Figure 1. Model of a generic linear noisy 2-port network. **(Left):** forward case. **(Right):** reverse case. The reverse case can be viewed as reversing the noisy thru and the noiseless 2-ports individually and then swapping them. It can be observed that: $Y_{S,NT} = Y_S$, $T_{eq,NT} = T_{eq}$; $Y'_{S,NT} = Y'_{out}$, $T'_{eq,NT} = T'_{out} - T_S G'_{av}$.

Now focus for a moment on the noisy thru (NT) alone. The relation between the equivalent noise temperature of the noisy thru and the elements of its (normalized) correlation matrix can be expressed as follows:

$$\frac{T_{eq,NT}}{T_0} \cdot G_{S,NT} = |Y_{S,NT}|^2 \hat{c}_{11} + 2G_{S,NT} \text{Re}[\hat{c}_{12}] - 2B_{S,NT} \text{Im}[\hat{c}_{12}] + \hat{c}_{22} . \quad (5)$$

Reversing the noisy thru yields another noisy thru, differing in the orientation of the noise generator and, therefore, with opposite correlation admittance:

$$e'_n = -e_n \quad (6)$$

$$i'_n = i_n \quad (7)$$

$$Y'_\gamma = -Y_\gamma , \quad (8)$$

where primes denote in this work the reverse mode. Thus, the correlation matrix of the reversed noisy thru is analogous to that of the original one, but with opposite terms in the secondary diagonal. Consequently, the equivalent noise temperature of the reversed noisy thru, $T'_{eq,NS'}$, can be expressed as:

$$\frac{T'_{eq,NT}}{T_0} \cdot G_{S,NT} = |Y_{S,NT}|^2 \hat{c}_{11} - 2G_{S,NT} \text{Re}[\hat{c}_{12}] + 2B_{S,NT} \text{Im}[\hat{c}_{12}] + \hat{c}_{22} , \quad (9)$$

where the elements of the correlation matrix are those of the original (i.e., forward) noisy thru, so they are not primed.

From these premises, it is easily shown that a consistent set of equations can be written down for the original 2-port, associated both with forward and reverse noise measurements. In particular, in the forward case, equations in the same form as (5) can be written down for various choices of the source admittance, since cascading the noiseless 2-port behind the noisy thru does not alter the equivalent noise temperature. Since cold-source measurements [18] will be considered in this work, (5) is rewritten to make explicit the role of the directly measured quantities, i.e., T_{out} and G_{av} :

$$\frac{T_{eq,NT}}{T_0} \cdot G_S = \frac{T_{out}/G_{av} - T_S}{T_0} \cdot G_S = |Y_S|^2 \hat{c}_{11} + 2G_S \text{Re}[\hat{c}_{12}] - 2B_S \text{Im}[\hat{c}_{12}] + \hat{c}_{22} . \quad (10)$$

As to the reverse case, the relevant configuration comprises the small-signal parameters of the reversed noiseless 2-port and the reversed noisy thru: see right side of Figure 1.

Therefore, equations such as (9) can be written, provided that the reference section is set between the noiseless and noisy subnetworks (section *s-Ri* in the scheme). Namely:

$$\frac{T'_{eq,NT}}{T_0} \cdot G'_{out} = \frac{T'_{out} - T_S G'_{av}}{T_0} \cdot G'_{out} = |Y'_{out}|^2 \hat{c}_{11} - 2G'_{out} \text{Re}[\hat{c}_{12}] + 2B'_{out} \text{Im}[\hat{c}_{12}] + \hat{c}_{22} \quad (11)$$

From a mathematical standpoint, any set of 4 linearly independent equations obtained from forward and reverse measurements over different terminations is sufficient to determine the unknown terms \hat{c}_{11} , $\text{Re}[\hat{c}_{12}]$, $\text{Im}[\hat{c}_{12}]$, \hat{c}_{22} . (In practice, reverse measurements are typically less reliable and are mainly used to give some redundancy. When measuring a transistor with the cold-source method, this is mainly because, the more unidirectional the device, the more compressed the range of its Y'_{out} admittances and T'_{out} noise temperatures.) Also, it is convenient to exploit a number of equations much larger than 4 to reduce the overall uncertainty. Solving the resulting over-determined system of linear equations is straightforwardly accomplished, for instance, by pseudo-inversion [28]. To this goal, (10) and (11) are first to be cast in matrix form, as follows:

$$\mathbf{b} = \mathbf{A} \cdot \mathbf{x} \quad (12)$$

$$\mathbf{b} = \begin{bmatrix} \vdots \\ \frac{T_{out,l}/G_{av,l} - T_{S,l}}{T_0} \cdot G_{S,l} \\ \vdots \\ \frac{T'_{out,m} - T_S G'_{av,m}}{T_0} \cdot G'_{out,m} \\ \vdots \end{bmatrix} \quad (13)$$

$$\mathbf{A} = \begin{bmatrix} \vdots & \vdots & \vdots & \vdots \\ |Y_{S,l}|^2 & +2G_{S,l} & -2B_{S,l} & 1 \\ \vdots & \vdots & \vdots & \vdots \\ |Y'_{out,m}|^2 & -2G'_{out,m} & +2B'_{out,m} & 1 \\ \vdots & \vdots & \vdots & \vdots \end{bmatrix} \quad (14)$$

$$\mathbf{x} = \begin{bmatrix} \hat{c}_{11} \\ \text{Re}[\hat{c}_{12}] \\ \text{Im}[\hat{c}_{12}] \\ \hat{c}_{22} \end{bmatrix}, \quad (15)$$

where $l = 1, 2, \dots, L$ and $m = 1, 2, \dots, M$ identify each termination condition in forward and reverse configuration, respectively. Another index $n = 1, 2, \dots, L, L + 1, L + 2, \dots, L + M = N$ can also be established to identify each equation independently of the configuration. Notice that the first L equations are equivalent to the classic solution proposed by Lane [7,11,29] while the additional M equations generalize the solution to using both forward and reverse measurements.

2.2. Proposed Test Bench

In order to build up the solving system, a suitable test bench needs to be set up to produce the measurement data. The architecture proposed in this contribution is shown in Figure 2 and allows to carry out cold-source measurements with online receiver calibration and measurement of the device under test (DUT)'s small-signal parameters. By replacing one of the terminations with a noise source, the Y-factor method may also be applied [18]: however, this possibility will not be considered in this work and the four terminations TERM0 through TERM3 will be assumed passive and at ambient temperature. In the following, the three possible configurations of the test bench are detailed:

- **Small-signal:** the SPMT switch is set so as to connect the thow to the VNA's port 1; the DPDT switch is set to vertical connections.
- **Pre-characterization:** the SPMT switch is set so as to connect the thow to one of the terminations; the DPDT switch is set to vertical connections.
- **Noise calibration:** the DPDT switch is set to vertical connections.
- **Noise measurement:** the SPMT switch is set so as to connect the thow to one of the terminations; the DPDT switch is set to horizontal connections.

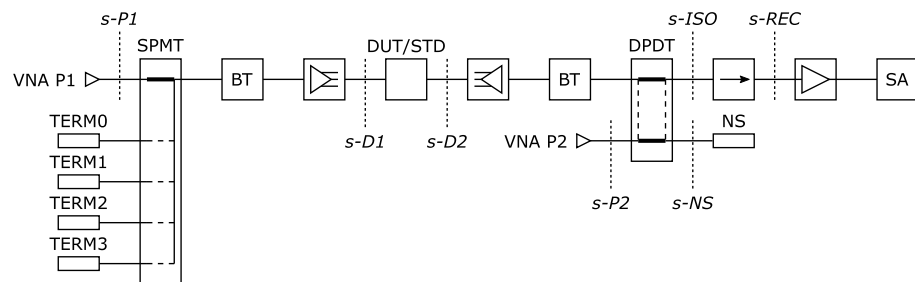


Figure 2. Block diagram of the cold-source noise test bench. From the left to the right along the noise measurement chain: cold (variable) terminations, SPMT switch, input bias-T, input RF probe, DUT or TRL standard, output RF probe, output bias-T, DPDT switch, ferrite isolator, pre-amplifier, spectrum analyzer. In addition, the SPMT is connected to the VNA's port 1 while the DPDT switch is in connected to a solid-state noise source and to the VNA's port 2. The SPMT switch is actually realized by combining a SP4T switch and a DPDT switch.

The first configuration is common to small-signal calibration and measurement. The only, obvious difference is that either calibration standards or the DUT are placed between sections $s-D1$ and $s-D2$. Whereas the calibration is performed once as the first step of the measurement campaign, the DUT will be repeatedly measured, i.e., in conjunction with the selection of each termination. In this work, a thru-reflect-line (TRL) calibration was performed, with custom on-wafer standards replicating exactly the access structures of the DUT. Thus, the DUT's reference planes were easily set in correspondence with the center section of the physical 'thru' standard.

The second configuration is used to characterize the source loads seen by the DUT. To ensure consistency, the same calibration performed in configuration 1 is exploited. Since the reference planes are at the center of the physical 'thru' standard, the measured S_{22} coincides with the sought-for Γ_S associated with the selected termination.

The third configuration allows to acquire two noise power readings from the receiver (from section $s-REC$ rightwards), relevant to the cold and hot states of the solid-state noise source. To that end, notice, the noise source's noise temperatures must be shifted to section $s-REC$ [23]. In turn, this requires an accurate knowledge of the passive network (BLK0) interposed between section $s-NS$ and section $s-REC$.

The fourth configuration allows the actual noise measurement. Specifically, a noise power reading is acquired, associated with the selected termination. Notice that the receiver's noise factor and gain are nominally the same as in the third configuration, due to the presence of a common isolator just ahead of section $s-REC$. Similar to the calibration step, processing the reading will require knowledge of the passive network (BLK2) interposed between section $s-D2$ and $s-REC$.

The small-signal parameters of the isolator alone and of the whole BLK0 are assumed to be known by way of a dedicated coaxial calibration. As to BLK2, it can be characterized as follows. First, apply the 'adapter removal' technique with a coaxial first tier at sections $s-P1$ and $s-ISO$ and an on-wafer second tier at sections $s-D1$ and $s-D2$. The result will be the scattering parameters of the passive network between sections $s-P1$ and $s-D1$ (BLK1) and of the passive network between sections $s-D2$ and $s-ISO$. Cascading the latter to the small-signal parameters of the isolator will yield the sought-for characterization of BLK2. Notice that BLK1, as a 2-port, is not needed in the cold-source approach, since characterizing the

DUT's source reflection coefficient (see description of configuration 2) is sufficient. If the Y-factor method were applied, however, steps similar to those just outlined would come in handy.

2.3. Precautions for Accuracy

As observed in [23], it is crucial that the parameters of all blocks remain stable during the measurement. For this reason, all passive blocks comprising flexible cables are kept mechanically fixed from their characterization onward. As to the variation of the DUT's source reflection coefficients, this is accomplished by controlling electro-mechanical switches as opposed to a tuner, to ensure repeatability. Clearly, the actual reflectances are measured directly at section $s-D1$, with the same on-wafer calibration used to measure the DUT.

Instabilities of the DUT's operating point are minimized by fixing its drain voltage and tuning the gate voltage so as to obtain a desired drain current. After selecting one of the source terminations and before sweeping in frequency the relevant noise measurement, the gate voltage is retuned and the DUT's scattering parameters remeasured. Also, every frequency point of the noise measurement is preceded by a retuning of the gate voltage. To ensure consistency of the bias points between forward and reverse measurements, 4-wire DC measurements are performed at the end of the cables connecting the supply/measurement unit (SMU) and the RF-decoupled port of the bias-T's. Then, the residual resistances of the bias-T's are measured and accounted for.

As to the receiver, this is made up of a pair of pre-amplifiers and a spectrum analyzer. The pre-amplifiers are necessary to increase the sensitivity of the whole receiver, but their total gain should be limited, both to avoid saturation and to limit gain instability. To remedy the instability of the receiver, the spectrum analyzer is made to auto-calibrate before each frequency sweep. Moreover, each noise power reading is accompanied by two readings for calibration. Also, each cycle of the DPDT switch is actually exploited for two sets of readings at the same frequency (calibration-cold, calibration-hot, measurement-cold, measurement-hot, calibration-cold, calibration-hot).

Ambient temperature is kept as constant as possible by air conditioning of the test laboratory. Contact of the probes is safeguarded from vibration by means of an anti-vibration table.

Finally, the resolution bandwidth (RBW) of the spectrum analyzer is limited to 0.8 MHz to ensure that the DUT's source reflection coefficient, Γ_S , remains sufficiently constant across the RBW itself. In this regard, Γ_S exhibits an angular variation with frequency of approximately 1 deg/MHz, as mainly due to the length of the cable between the SPMT and the input bias-T. As to the video bandwidth (VBW), it is set to 20 Hz to improve the stability of the readings. As a further measure, 101 point traces are acquired and averaged at each reading.

2.4. De-Embedding and Processing

Provided that the isolator in front of the receiver is sufficiently unidirectional, the nominal parameters of the receiver (REC) are common to the three noise power readings taken in the calibration and measurement steps:

$$N_{c,cal} = k_B (T_{c,cal} + T_{eq,REC}) B G_{av,REC} \quad (16)$$

$$N_{h,cal} = k_B (T_{h,cal} + T_{eq,REC}) B G_{av,REC} \quad (17)$$

$$N_{c,msm} = k_B (T_{c,msm} + T_{eq,REC}) B G_{av,REC} , \quad (18)$$

where $T_{c,cal}$, $T_{h,cal}$ and $T_{c,msm}$ are all referred to section $s-REC$:

$$T_{c,cal} = T_{c,NS} G_{av,BLK0} \quad (19)$$

$$T_{h,cal} = T_{h,NS} G_{av,BLK0} \quad (20)$$

$$T_{c,msm} = T_{out} G_{av,BLK2} . \quad (21)$$

By linear interpolation/extrapolation, it is easily found that:

$$T_{c,msm} = T_{c,cal} + (N_{c,msm} - N_{c,cal}) \cdot \frac{T_{h,cal} - T_{c,cal}}{N_{h,cal} - N_{c,cal}}, \quad (22)$$

from which BLK2 is straightforwardly de-embedded by inverting (21). Then, (10) and (11) or, equivalently, (12)–(15) can be written down and solved by pseudo-inversion, as discussed in Section 2.1.

Adopting both forward and reverse noise measurements allows to build up an over-determined system of equations, which improves the quality of the extractions. However, only a total of $N = 8$ equations is reached in this manner, which is still quite scarce as compared to a typical value of a few tens. Also, there is in practice no control on the actual spread of the terminations resulting at each measurement frequency. To the contrary, well spread termination patterns will result at some frequencies and not at others, easily leading to a rapid succession of good and bad extractions.

To mitigate this issue, the Authors suggest extending the input data for each nominal frequency to the set of all measurements in its neighborhood. The idea is similar to what proposed in [16,17], where a long transmission line is exploited at the input of the transistor under test. The present problem, however, has to tackle very long electrical paths which are not necessarily good approximations of transmission lines.

Under these conditions, it can be assumed that, whereas the DUT's source reflection coefficients vary significantly from one frequency to another (with a frequency step of 100 MHz), the elements of the DUT's correlation matrix can be safely approximated to the first-order at frequencies f in a neighborhood $[f_1, f_2]$ of a nominal frequency f_0 . This corresponds to modifying \mathbf{A} and \mathbf{x} of (14) and (15) into their 'expanded' counterparts:

$$\mathbf{A}_e = \begin{bmatrix} \vdots & \vdots \\ a_{n,1} & a_{n,1}\Delta f & a_{n,2} & a_{n,2}\Delta f & a_{n,3} & a_{n,3}\Delta f & a_{n,4} & a_{n,4}\Delta f \\ \vdots & \vdots \end{bmatrix} \quad (23)$$

$$\mathbf{x}_e = \begin{bmatrix} x_{1,0} \\ x_{1,1} \\ x_{2,0} \\ x_{2,1} \\ x_{3,0} \\ x_{3,1} \\ x_{4,0} \\ x_{4,1} \end{bmatrix}, \quad (24)$$

where $\Delta f = f - f_0$ and $x_i \approx x_{i,0} + x_{i,1}\Delta f$. Thus, system (12) is transformed to:

$$\mathbf{b} = \mathbf{A}_e \cdot \mathbf{x}_e. \quad (25)$$

Obviously, here vector \mathbf{b} does not undergo any formal modification with respect to (12) and (13), but its elements will be associated with a larger set of frequency points.

As the breadth $B_L = f_2 - f_1$ of the interval $[f_1, f_2]$ is enlarged, more and more frequency points will fall within it, each contributing with additional 8 equations. Of course, dilating that interval indefinitely would contrast with the hypothesis that the terms of \mathbf{x} can be linearized in f_0 between f_1 and f_2 . Another possible issue with this approach is that measurements affected by pathological problems (e.g., badly characterized block, failed reading) at some single frequencies will extend their detrimental effects to the nearby frequencies too. Therefore, a critical comparison of the standard and expanded solutions should be performed.

3. Results

The noise measurement approach presented in Section 2 was tested on an active device fabricated by OMMIC on its recently developed 60 nm gate length GaN-on-Si HEMT technology (D006GH). The device has 4 fingers of 35 μm unit gate width. The reference operating point is $V_{DS} = 5\text{ V}$, $I_D = 17.1\text{ mA}$, which was believed to be approximately optimum for noise performance. Other drain currents were also tested to confirm that hypothesis.

The measurement frequency range was set from 20 GHz to 40 GHz, with a 100 MHz step. As anticipated in Section 2, 4 physical terminations were adopted, which yield 8 measurements per frequency point since both the forward and the reverse modes were exploited. As expected, this number is still too low to ensure a reliable extraction of the noise parameters at all frequencies. Indeed, the extracted elements of the correlation matrix, shown with dashed lines of Figure 3, are often unphysical. Pruning the unphysical points from these extractions yields the continuous thin lines in the same figure.

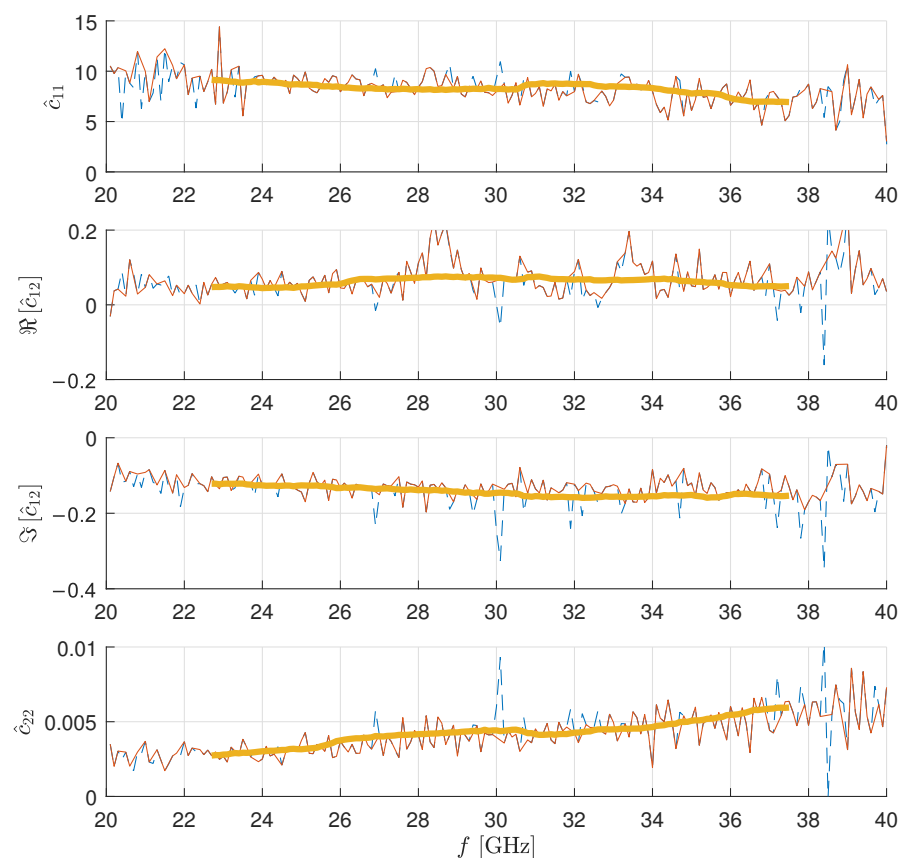


Figure 3. Extraction of the elements of the noise correlation matrix over frequency. Dashed lines: standard extraction ($f_1 = f_0 = f_2$). Continuous thin lines: physically sound subset of the standard extraction. Continuous thick lines: linearization-based extraction ($f_1 = f_0 - 2.5\text{ GHz}$, $f_2 = f_0 + 2.5\text{ GHz}$).

Therefore, the linearization-based method illustrated in Section 2.4 was employed to improve the extraction. Observing the pruned traces in Figure 3 justifies the selection of a frequency interval B_L up to a few gigahertz. However, increasing B_L also entails a reduction of the measurement frequency range at either end. Therefore, $B_L = 5\text{ GHz}$ was set (i.e., $f_1 = f_0 - 2.5\text{ GHz}$, $f_2 = f_0 + 2.5\text{ GHz}$). The result is shown by the continuous thick lines in Figure 3.

Notice that the linearization-based traces are similar to what could be obtained by smoothing or fitting the pruned traces of the standard extraction. However, the proposed approach exhibits the following advantages:

- Rather than discarding the data at frequencies where the standard extraction fails, it produces a reliable extraction at a certain frequency f_0 by merging all data at nearby frequencies. This may be especially beneficial when the single-frequency failures are numerous.
- As compared to fitting, it does not assume any particular model, but only that the elements of the correlation matrix can be linearized.

The noise correlation matrix can be converted to the more familiar noise parameters through well known formulae. For the Reader's convenience, it is worth recalling that:

$$R_n = \hat{c}_{11} \quad (26)$$

$$Y_{opt} = \sqrt{\frac{\hat{c}_{22}}{\hat{c}_{11}} - \left(\text{Im}\left[\frac{\hat{c}_{12}}{\hat{c}_{11}}\right]\right)^2} + j\text{Im}\left[\frac{\hat{c}_{12}}{\hat{c}_{11}}\right] \quad (27)$$

$$F_{min} = 1 + 2\left(\hat{c}_{12} + R_n Y_{opt}^*\right) \quad (28)$$

as well as that, in general:

$$\Gamma = \frac{Y_0 + Y}{Y_0 - Y} \quad (29)$$

$$NF = 10 \log(F) \text{ [dB]}, \quad (30)$$

with $Y_0 = 1/Z_0$ the normalization admittance and Z_0 the normalization impedance (typically 50 Ω).

The noise parameters corresponding to the pruned traces of Figure 3 are shown in Figure 4 as isolated points. Then, two linearization-based extractions are also shown, associated with two different values of B_L , namely 1 GHz (continuous thin lines) and 5 GHz (continuous thick lines). It is interesting to notice that the extraction adopting $B_L = 1$ GHz is much smoother than the standard extraction; however, a problematic hump in NF_{min} in the 28–29 GHz frequency range is found (which, incidentally, appears strongly correlated to the small-signal parameters of blocks BLK2 and BLK0 at those frequencies). Increasing B_L up to 5 GHz further irons out all traces.

The effect of increasing B_L , as mentioned in Section 2.4 consists in allowing more source (in forward mode) and output (in reverse mode) terminations to contribute to each extraction. As an example, the extractions at $f_0 = 35$ GHz with $B_L = 1$ GHz and $B_L = 5$ GHz are shown in Figure 5. It is evident that the number of terminations and their spreading across the reflectance plane improves significantly with higher and higher values of B_L .

To further illustrate this effect, extractions with different settings are compared in Table 1 at the target frequency $f_0 = 35$ GHz (a nearby frequency is shown when the extraction fails at 35 GHz). In particular, the first three columns present the extraction failure rate versus B_L and the exploited configuration. The term 'failure rate' here denotes the ratio of the number of frequencies associated with physically sensible extractions to the total number. It is evident that in the given scenario the failure rate drops to very low values, even with moderate bandwidths ($B_L \geq 0.5$ GHz), when both forward (FWD) and reverse (RVS) configurations are adopted. The remaining columns provide the actual frequency and the extracted noise parameters.

Among the considered settings, notice that those presented in the last row of Table 1 correspond to a standard source-pull approach with the minimum number of terminations. Similarly, the third row corresponds to a semi-standard approach exploiting both source- and load-pull data. Thus, these two rows can serve as a familiar term of comparison for the full-blown methodology presented in this contribution.

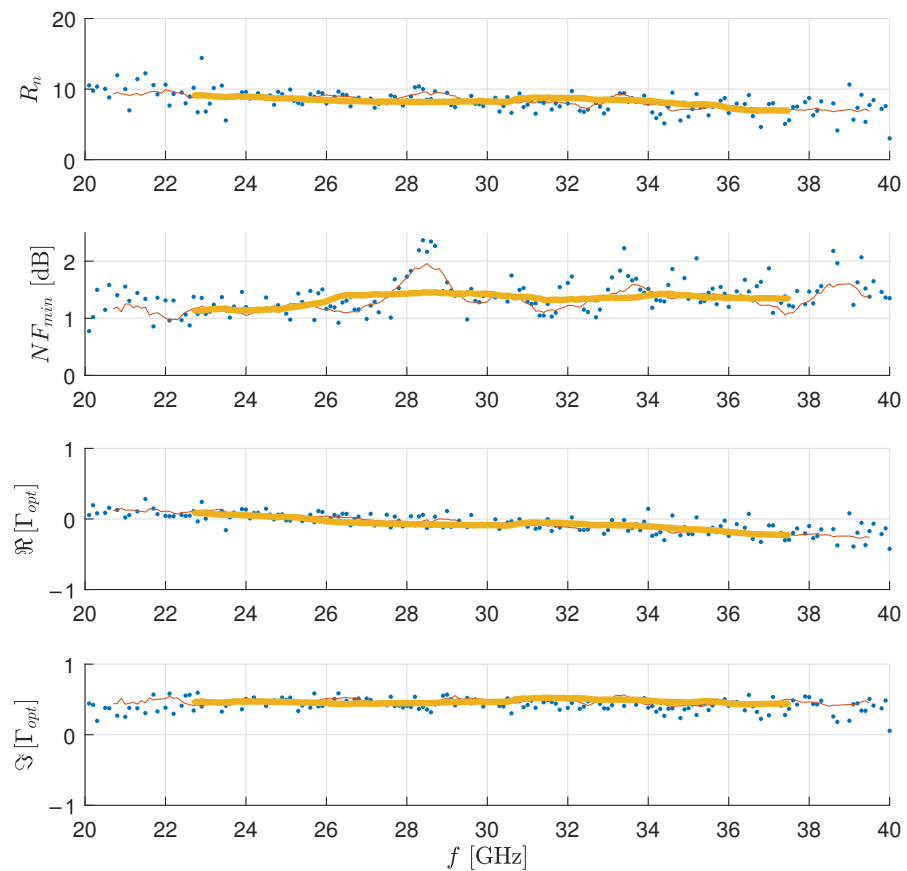


Figure 4. Conversion of the noise correlation matrix to the noise parameters over frequency. Points: physically sound subset of the standard extraction. Continuous thin lines: linearization-based extraction ($f_1 = f_0 - 0.5$ GHz, $f_2 = f_0 + 0.5$ GHz). Continuous thick lines: linearization-based extraction ($f_1 = f_0 - 2.5$ GHz, $f_2 = f_0 + 2.5$ GHz).

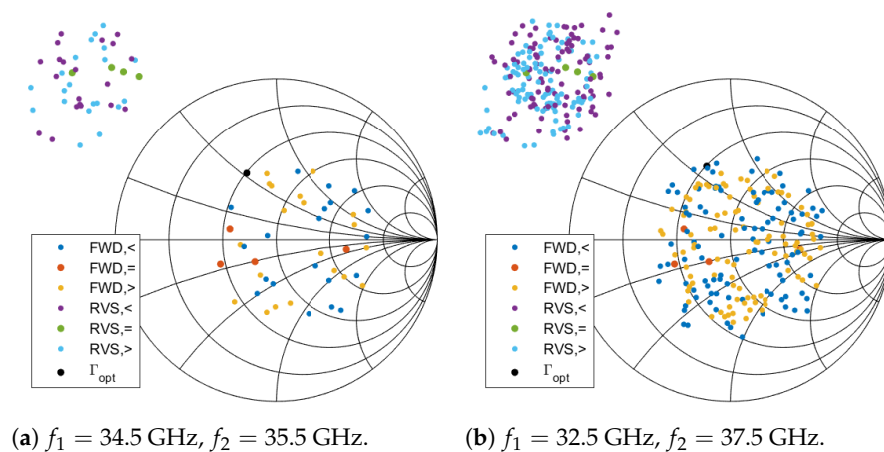


Figure 5. Example of termination pattern for the extraction of the noise parameters at $f_0 = 35$ GHz. The terminations form groups depending whether they are associated with frequencies lower than f_0 (<), equal to f_0 (=) or higher than f_0 (>), and whether they refer to the forward (FWD) or reverse (RVS) mode. In this particular case, the forward mode Γ_S reflectances and the reverse mode Γ'_{out} reflectances happen to be inside and outside of the passive Smith chart, respectively. The black point represents the optimum point Γ_{opt} .

Although the data in Table 1, being referred to one single target frequency, can only give an incomplete picture of the state of affairs, nevertheless they allow to illustrate some

overall trends. First of all, the 4-termination standard approach (row 6) is seen to be unreliable in this case: besides an unsatisfactory failure rate, the noise parameters which it yields are quite off as compared to the the first four rows. This situation improves only slightly for row 5, which approximately corresponds to a standard approach with a higher number of source terminations. Broadening B_L further, as in row 4, still results in a mediocre failure rate; however, the noise parameters now get to yield, together with the first three rows, a consistent bulk of extractions.

Merging source- and load-pull data in one single extraction seems to produce generally good results with all choices of B_L , and in particular even with $B_L = 0$ GHz [10], as in row 3. However, larger and larger bandwidths B_L also yield smoother traces and considerably lower failure rates, as in rows 2 and 1.

Table 1. Comparison among different extraction settings.

B_L [GHz]	Configurations	Failure Rate [%]	f_0 [GHz]	NF [dB]	R_n [Ω]	$ \Gamma_{opt} $	$\angle\Gamma_{opt}$ [rad]
2.5	FWD + RVS	0.67	35	1.41	7.78	0.48	1.88
0.5	FWD + RVS	2.68	35	1.36	7.09	0.45	1.99
0	FWD + RVS	19.46	35	1.34	6.09	0.43	2.08
2.5	FWD	42.95	35	1.40	7.50	0.53	1.79
0.5	FWD	42.28	35.5	1.16	5.25	0.60	1.87
0	FWD	32.21	35.1	1.50	16.01	0.23	1.58

In addition to the reference drain current $I_D = 17.1$ mA, similar extractions were performed at other current values, namely 34.2 mA, 51.2 mA and 68.3 mA. The resulting noise parameters are shown in Figure 6. A noticeable difference is found in particular among the extracted traces of R_n and NF_{min} , with a clear trend towards higher values for drain currents from 34.2 mA up. The first two values of drain current lead to very similar results, indicating that the optimum operation must lie somewhere in between.

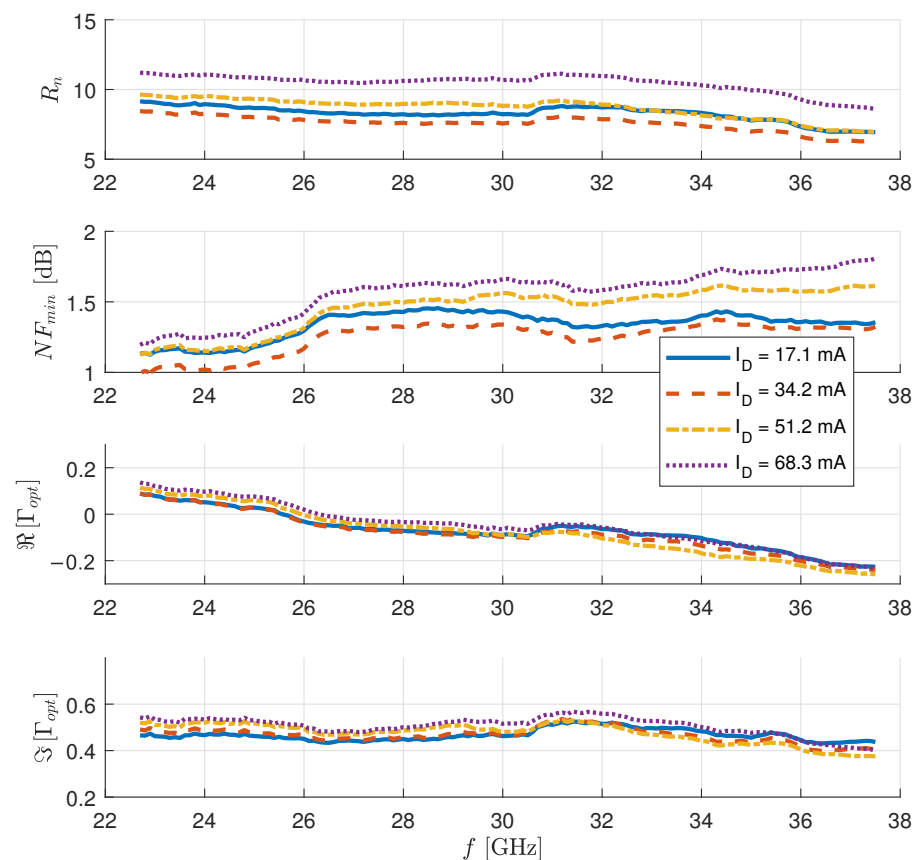


Figure 6. Extracted noise parameters over frequency at different current values.

Finally, the black-box characterization of the active device was inserted in the simulation of a mixed-technology low-noise amplifier already described in [22]. Whereas the last three stages of the amplifier are based on 100 nm devices, the first stage features a 60 nm transistor with the same geometry considered above, i.e., $4 \times 35 \mu\text{m}$. As can be seen from Figure 7, the noise figure simulated in this manner compares well with the actual measurement performed on the realized amplifier. However, the latter is a classical Y-factor measurement (not corrected for the imperfect match of the source termination), whereas the simulation is referred to a perfect 50Ω resistance.

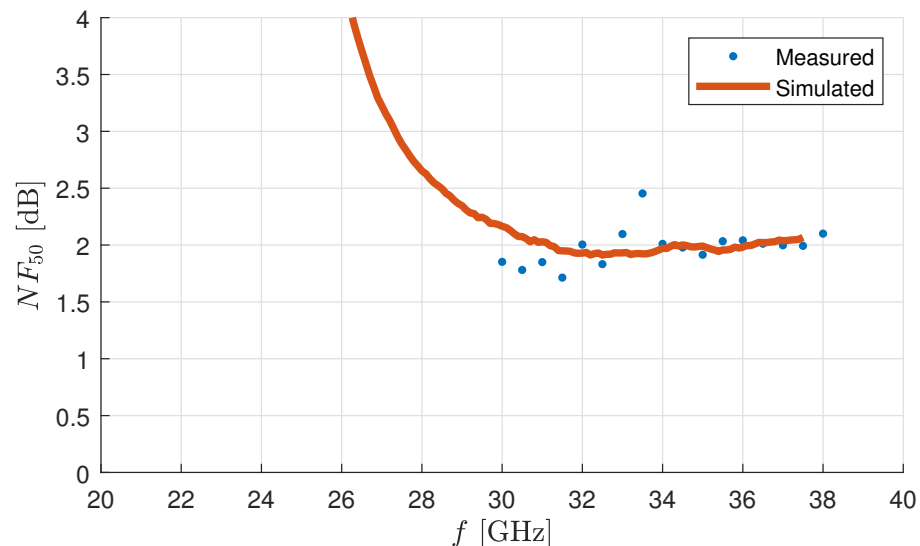


Figure 7. Noise figure of the mixed-technology LNA from [22]. The measurement refers to the actual, realized amplifier. The simulation is obtained by using the black-box characterization to simulate the first stage. The other stages are in the 100 nm technology and maintain their previous models.

4. Discussion

As anticipated in the Introduction, the proposed black-box characterization approach blends together several ideas which have been around for some time, namely, the use of electro-mechanical switches rather than of tuners; the exploitation of both forward and reverse modes; the combination of measurements at multiple frequencies into single-frequency extractions. Out of these, the last is probably the most effective in producing robust results.

In this respect, it is worth reappraising the observation, already made in the Introduction, that typical black-box approaches require several physical terminations in order to allow an extraction of the four noise parameters at one frequency. In the light of the presented linearization-based technique, that statement loses validity in the present case: mathematically, the adopted first-order approximation of the noise correlation matrix allows for as few as one single physical termination. (Indeed, the Authors have found that reasonable extractions can be obtained with one physical termination only, although at the cost of increasing B_L significantly.)

Leaving now aside the mathematical foundation of the approach, the present implementation of the test bench also deserves some comments. In the Authors' opinion, the results presented in Section 3 are very encouraging. However, significant room for improvement can be found.

First of all, the present version of the test bench, mainly set up as a proof of concept, has not been optimized yet with respect to the hardware side. In particular, the coaxial cables connecting the switches with the bias-T's are of mediocre quality, which results in significant loss in key paths of the measurement chain. As can be seen in Figure 5, the maximum magnitude of the source reflectances synthesized at section $s-D1$ is rather poor, as due to the excessive loss of the input cable. On the other hand, the loss of the output

cable impacts negatively on BLK2 and, ultimately, on the uncertainty associated with the single noise measurements. It is thus imperative to reduce in length and improve in quality those two cables in the future.

Moreover, it should be further investigated whether or not the implemented algorithm for tuning the operating point can ensure sufficient stability of the DUT's behavior. If so, the online measurement of the DUT's small-signal parameters could be spared, with obvious beneficial effects on the setup architecture. For instance, it would be possible to reallocate section *s-P1* to one further termination. Alternatively, although at the cost of manually switching the source terminations, the input switch could be eliminated altogether, and the input cable with it.

5. Conclusions

A new approach to the black-box noise characterization of active devices has been proposed and a cold-source test bench suitable to its application has been presented. The approach conveniently combines in a single, coherent workflow several ideas which, taken separately, are already in use in the measurement practice oriented to high-frequency electronic circuits. The validity of the extraction technique has been demonstrated through a characterization campaign of a HEMT device from an advanced 60 nm GaN-on-Si MMIC technology. The current weaknesses and future developments of the cold-source test bench are also discussed.

Author Contributions: Conceptualization, S.C. and W.C.; methodology, S.C. and W.C.; software, S.C.; validation, S.C., W.C., L.P., P.E.L. and A.S.; formal analysis, S.C. and A.S.; resources, J.P. and R.L.; data curation, S.C. and W.C.; writing—original draft preparation, S.C.; writing—review and editing, S.C. and P.E.L.; supervision, E.L.; project administration, E.L.; funding acquisition, E.L. All authors have read and agreed to the published version of the manuscript.

Funding: This research and the APC were funded by the European Union under project H2020-COMPET-2017 MiGANSOS, grant number 776322.

Institutional Review Board Statement: Not applicable.

Informed Consent Statement: Not applicable.

Data Availability Statement: Not applicable.

Conflicts of Interest: The authors declare no conflict of interests. The funders had no role in the design of the study; in the collection, analyses, or interpretation of data; in the writing of the manuscript, or in the decision to publish the results.

Sample Availability: Samples are to be requested to the foundry.

Abbreviations

The following abbreviations are used in this manuscript:

SAR	Synthetic-Aperture Radar
SCFE	Single-Chip Front End
MMIC	Monolithic Microwave Integrated Circuit
HEMT	High-Electron Mobility Transistor
GaN	Gallium Nitride
Si	Silicon
DC	Direct Current
RF	Radio Frequency
NT	Noisy Thru
NS	Noise Source
TERM	Termination
DUT	Device Under Test
STD	Standard (of calibration kit)
SPMT	Single-Pole Multiple-Throw
DPDT	Double-Pole Double-Throw

BLK	Block (i.e., passive block of measurement chain)
REC	Receiver
FWD	Forward
RVS	Reverse
SMU	Supply/Measure Unit
VNA	Vector Network Analyzer
TRL	Thru-Reflect-Line
SA	Spectrum Analyzer
RBW	Resolution Bandwidth
VBW	Video Bandwidth

References

- Engberg, J.; Larsen, T. *Noise Theory of Linear and Nonlinear Circuits*; John Wiley & Sons, Ltd.: Chichester, UK, 1995.
- Rothe, H.; Dahlke, W. Theory of Noisy Fourpoles. *Proc. IRE* **1956**, *44*, 811–818, doi:10.1109/JRPROC.1956.274998.
- Pucel, R.A.; Haus, H.A.; Statz, H. Signal and noise properties of Gallium Arsenide microwave field-effect transistors. *Adv. Electron. Electron Phys.* **1975**, *38*, 195–265.
- Pospieszalski, M.W. Modeling of noise parameters of MESFETs and MODFETs and their frequency and temperature dependence. *IEEE Trans. Microw. Theory Tech.* **1989**, *37*, 1340–1350, doi:10.1109/22.32217.
- Mokari, M.E.; Patience, W. A new method of noise parameter calculation using direct matrix analysis. *IEEE Trans. Circuits Syst. I Fundam. Theory Appl.* **1992**, *39*, 767–771, doi:10.1109/81.250168.
- Chusseau, L.; Parisot, M.; Jousseau, N. Automatic Full Noise Characterization of Microwave GaAs FETs. In Proceedings of the 1987 17th European Microwave Conference, Rome, Italy, 7–11 September 1987; pp. 628–632, doi:10.1109/EUMA.1987.333677.
- Lane, R.Q. The determination of device noise parameters. *Proc. IEEE* **1969**, *57*, 1461–1462, doi:10.1109/PROC.1969.7311.
- Wedge, S.; Rutledge, D. Wave techniques for noise modeling and measurement. *IEEE Trans. Microw. Theory Tech.* **1992**, *40*, 2004–2012, doi:10.1109/22.168757.
- Wait, D.; Engen, G. Application of Radiometry to the accurate measurement of amplifier noise. *IEEE Trans. Instrum. Meas.* **1991**, *40*, 433–437, doi:10.1109/TIM.1990.1032979.
- Ciccognani, W.; Colangeli, S.; Serino, A.; Longhi, P.E.; Limiti, E. Generalized Extraction of the Noise Parameters by Means of Source- and Load-Pull Noise Power Measurements. *IEEE Trans. Microw. Theory Tech.* **2018**, *66*, 2258–2264, doi:10.1109/TMTT.2018.2794995.
- Colangeli, S.; Ciccognani, W.; Palomba, M.; Limiti, E. Automated extraction of device noise parameters based on multi-frequency, source-pull data. *Int. J. Microw. Wirel. Technol.* **2014**, *6*, 63–72.
- Simpson, G.; Ballo, D.; Dunsmore, J.; Ganwani, A. A new noise parameter measurement method results in more than 100x speed improvement and enhanced measurement accuracy. In Proceedings of the 72nd ARFTG Microwave Measurement Symposium, Portland, OR, USA, 9–12 December 2008; pp. 119–127, doi:10.1109/ARFTG.2008.4804299.
- Randa, J. Amplifier and Transistor Noise-Parameter Measurements. In *Wiley Encyclopedia of Electrical and Electronics Engineering*; Webster, J., Ed.; John Wiley & Sons, Inc.: Chichester, UK, 2014. Available online: <https://onlinelibrary.wiley.com/doi/abs/10.1002/047134608X.W8219> (accessed on 7 September 2021).
- Randa, J. Comparison of noise-parameter measurement strategies: Simulation results for amplifiers. In Proceedings of the 84th ARFTG Microwave Measurement Conference, Boulder, CO, USA, 4–5 December 2014; pp. 1–8, doi:10.1109/ARFTG.2014.7013402.
- Randa, J. Simulator for amplifier and transistor noise-parameter measurements. In Proceedings of the CPEM 2010, Daejeon, Korea, 13–18 June 2010; pp. 555–556, doi:10.1109/CPEM.2010.5544823.
- Larock, V.; Meys, R. Automatic Noise Temperature Measurement through Frequency Variation. *IEEE Trans. Microw. Theory Tech.* **1982**, *30*, 1286–1288, doi:10.1109/TMTT.1982.1131242.
- Hu, R.; Weinreb, S. A novel wide-band noise-parameter measurement method and its cryogenic application. *IEEE Trans. Microw. Theory Tech.* **2004**, *52*, 1498–1507, doi:10.1109/TMTT.2004.827029.
- Tiemeijer, L.F.; Havens, R.J.; de Kort, R.; Scholten, A.J. Improved Y-factor method for wide-band on-wafer noise-parameter measurements. *IEEE Trans. Microw. Theory Tech.* **2005**, *53*, 2917–2925, doi:10.1109/TMTT.2005.854243.
- Gu, D.; Walker, D.K.; Randa, J. Noise-parameter measurement with automated variable terminations. In Proceedings of the 2008 Conference on Precision Electromagnetic Measurements Digest, Broomfield, CO, USA, 8–13 June 2008, pp. 706–707, doi:10.1109/CPEM.2008.4574975.
- OMMIC's Website. Available online: <https://www.ommic.com/iii-v-processes/> (accessed on 19 July 2021).
- CORDIS' Website on the MiGaNSOS Project. Available online: <https://cordis.europa.eu/project/id/776322/> (accessed on 19 July 2021).
- Pace, L.; Longhi, P.E.; Ciccognani, W.; Colangeli, S.; Leblanc, R.; Limiti, E. A MMIC Low-Noise Amplifier realized with two different gate length GaN-on-Si technologies. In Proceedings of the European Microwave Conference (EuMC), Utrecht, The Netherlands, 12–14 January 2021; pp. 1023–1026, doi:10.23919/EuMC48046.2021.9338196.
- Colangeli, S.; Ciccognani, W.; Longhi, P.E.; Pace, L.; Poulain, J.; Leblanc, R.; Limiti, E. Linear Characterization and Modeling of GaN-on-Si HEMT Technologies with 100 nm and 60 nm Gate Lengths. *Electronics* **2021**, *10*, 134, doi:10.3390/electronics10020134.

24. Venugopal, D.; Muthugadahalli, C.; K. S., M.; Narayanan, K. Ka band satellite communication systems—Applications and configurations. In Proceedings of the International Astronautical Congress, Jerusalem, Israel, 12–16 October 2015.
25. Ludwig, M.; Daganzo-Eusebio, E.; Davidson, M. Ka-Band radar missions for earth observation. In Proceedings of the 2013 IEEE International Geoscience and Remote Sensing Symposium—IGARSS, Melbourne, Australia, 21–26 July 2013; pp. 2289–2292, doi:10.1109/IGARSS.2013.6723275.
26. Pace, L.; Colangeli, S.; Ciccognani, W.; Longhi, P.E.; Limiti, E.; Leblanc, R.; Feudale, M.; Vitobello, F. Design and validation of 100 nm GaN-on-Si Ka-Band LNA based on custom noise and small signal models. *Electronics* **2020**, *9*, 150, doi:10.3390/electronics9010150.
27. Pace, L.; Costanzo, F.; Longhi, P.; Ciccognani, W.; Colangeli, S.; Suriani, A.; Leblanc, R.; Limiti, E. Design of a Ka-band single-chip front-end based on a 100 nm GaN-on-Si technology. In Proceedings of the Integrated Nonlinear Microwave and Millimetre-Wave Circuits Workshop (INMMiC), Cardiff, UK, 16–17 July 2020; doi:10.1109/INMMiC46721.2020.9160306.
28. Penrose, R. A generalized inverse for matrices. *Math. Proc. Camb. Philos. Soc.* **1955**, *51*, 406–413, doi:10.1017/S0305004100030401.
29. Colangeli, S.; Bentini, A.; Ciccognani, W.; Limiti, E. Polynomial noise modeling of Silicon-based GaN HEMTs. *Int. J. Numer. Model. Electron. Netw. Devices Fields* **2014**, *27*, 812–821, doi:10.1002/jnm.1907.